Modifying a "Mathematical Framework for Activity-Based Cancer Biomarkers":

Correlating Tumor Size and Reporter Concentration

Erik Bergstrom, Nathaniel Gutierrez, Helen Masson

BENG 221

December 11, 2017

Contents

1 Introduction

1.1 Background

1.1.1 Cancer

Cancer is the second leading cause of death in the United States [1]. According to the National Cancer Institute, approximately 39.6% of men and women will be diagnosed with cancer at some point during their lifetimes [2]. This complex disease takes many forms and has various underlying causes, contributing to its high death rate. Current forms of treatment involve therapies such as radiation and chemotherapy, which essentially act as a poison to kill the cancer cells causing severe side-effects for the patient. Other treatments include surgical removal of the tumor from the patient. These treatments are often combined to ensure complete removal of the cancer from the patient. The efficacy of these treatments is dependent on early detection of the disease. For the majority of cancer types, diagnosing the cancer when it is still localized in the organ of origin correlates with a greater long-term survival [3][4][5]. For this reason, there is a strong need to develop technologies that can detect cancer at an early stage of the disease. To accomplish this, one must have a deep understanding about the underlying biology and mechanisms of cancer.

Our bodies are comprised of over 37.2 trillion cells, and cancer can originate with a single genetically-altered cell essentially anywhere in the body [6]. The term "cancer" encompasses a collection of diseases characterized by uncontrollable cell division and abnormal cell invasion into surrounding tissues. The majority of cancers form stationary, solid tumors, however cancers of the blood (leukemias) typically circulate and affect the blood, bone marrow, and lymphoid system. Additionally, tumors can be either malignant or benign. Benign tumors do not invade surrounding tissue or spread to other parts of the body like cancerous malignant tumors.

Cancer cells are genetically and phenotypically different from normal cells of the body, and these differences are what allow them to grow out of control and become invasive. Douglas Hanahan and Robert A. Weinberg in "The Hallmarks of Cancer" state that there are 6 key differences that characterize all cancer cells (Figure 1): i) stimulated self-growth ii) resistance to inhibitory signals iii) resistance to programmed cell death (apoptosis) iv) limitless replicative potential v) induced formation of vasculature (angiogenesis) and vi) ability to invade surrounding tissues and spread to other sites in the body (metastasis) [7].
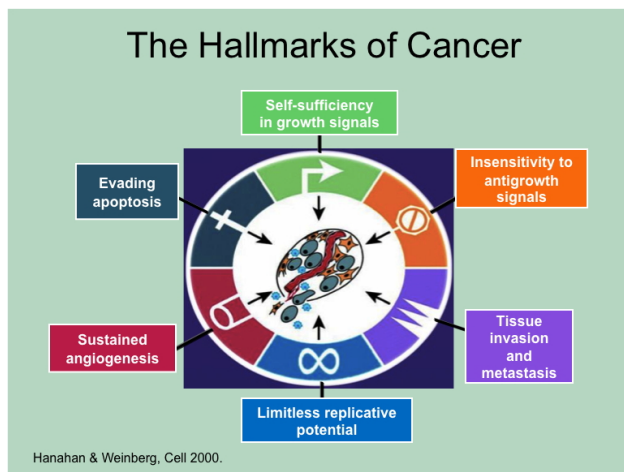

Figure 1: The 6 Hallmarks of Cancer. Image courtesy of Hanahan *et al*, 2011.

These hallmark differences between cancer cells and normal cells manifest themselves at the genetic and molecular level and serve as cancer biomarkers. Biomarkers are a measurable substance in an organism whose presence is indicative of some phenomenon such as disease, infection, or environmental exposure[8]. The clinical management of cancer is increasingly dependent on the discovery and development of novel biomarkers and ultrasensitive technologies to detect them at early stages when therapeutic intervention may

still be effective [9][10]. The biomarker used for this model and study is matrix mettaloproteinase 9 (MMP9). This enzyme is involved in the degradation and remodeling of the extracellular matrix, a fundamental role in tumor progression. MMP9 is highly expressed in cancer cells and contributes to their ability to metastasize (hallmark 6). Additionally, MMP9 was shown to be up-regulated across many different cancers (Figure 2).
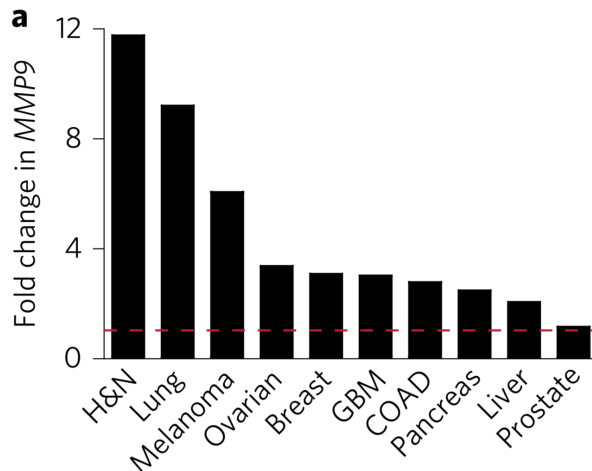

Figure 2: Analysis of fold change in MMP9 mRNA expression in tumors versus healthy controls; compiled from Oncomine and TCGA data. H&N, head and neck; GBM, glioblastoma multiforme; COAD, colorectal adenocarcinoma. Red dashed line indicates a fold change of 1. Image courtesy of Kwon *et al*, 2017.

Despite the need for sensitive diagnostic tools that are capable of detecting cancer at early stages of the disease, current biomarker technology has limited predictive value. For instance, screening with the blood biomarker CA-125 for ovarian cancer diagnosis does not improve patient outcome [11]. Current diagnostic strategies such as magnetic resonance imaging, positron emission tomography, and analysis of blood biomarkers shed by tumors are limited to the detection of masses 1cm in diameter[12][13][14]. It has been shown that it can take up to ten years for a tumor to reach this size [13], leaving a large window of opportunity for early diagnosis to enhance patient outcomes. The development of ultrasensitive, minimally invasive diagnostic tools could significantly improve patient prognosis[15].

1.1.2   Nanoparticle Biosensor

Ester Kwon and her group developed an exogenously administered activity-based nanosensor (ABN) as a minimally invasive technique for detecting tumors [15]. The ABN is designed to effectively diffuse out of the plasma into the tumor after injection. Once concentrated in the tumor, the particle will shed a reporter molecule that is cleaved from tumor-specific proteases. This reporter diffuses back into the blood and will ultimately concentrate in the urine for quantification (Figure 3).

Kwon optimized the transport of the particle into tumor tissue by conjugating LyP-1 to the surface. This substrate recognizes membrane-bound receptors on the surface of tumor cells and initiates an active transport mechanism, allowing the ABN to diffuse into the tissue. The ABN was also optimized to recognize on-target proteases by lengthening the MMP substrate that is also attached to the nanoparticle core. Increasing the length of the substrate caused the off-target protease activity to decrease.
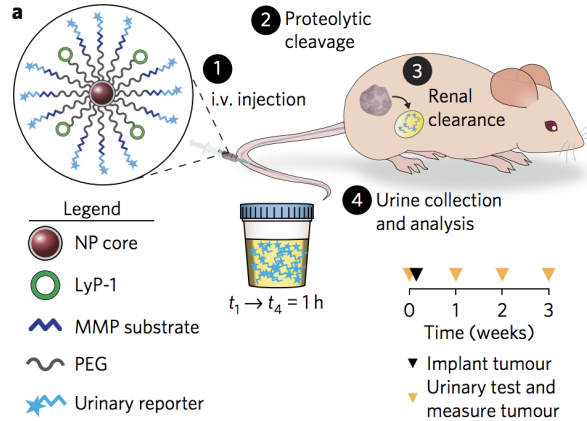
Figure 3: Schematic of tumor detection using the nanoparticle system. The process is broken into four steps; 1) Injection of the nanoparticle 2) Proteolytic cleavage of the MMP substrate and reporter 3) Clearance of the reporter in the kidneys 4) Collection of the reporter in the urine. Image courtesy of Kwon, *et al*, 2017.

1.2   Problem Statement

The efficacy of cancer therapeutics is dependent on early detection of the disease. Current biomarker technologies do not have the predictive value to diagnose cancer at early enough stages to have a positive effect on patient prognosis. Current imaging and blood biomarker technologies are limited to detecting masses with a minimum diameter of 1cm (it can take up to 10 years for a tumor to reach that size). Additionally, current biosensor models have no way of predicting or monitoring tumor size.

Dr. Ester Kwon and team have engineered an ultra-sensitive tumor penetrating nanosensor that can detect sub-5mm-tumors, however the model does not include a means of measuring tumor size. Here, we attempt to modify the mathematical model of her activity-based nanosensor to incorporate a measure of tumor size. We hypothesize that concentration of the cleavable reporter in urine will increase as tumor size increases.

2   Methods

2.1   Lumped Model

To develop a mathematical model for the activity of the nanoparticle in a living system, Kwong *et al* broke the system into a lumped model consisting of four compartments (Figure 4). The first compartment represents the concentration of the NPs in the blood after injection. The second compartment represents the concentration of the NPs in the tumor. The third compartment represents the concentration of the cleaved reporter in the blood. The fourth compartment represents the concentration of reporter that accumulates in the bladder and urine. The model also includes an additional pathway that depicts the proteolytic cleavage that occurs within the plasma from both on and off-target enzymes. Table 1 below lists the values for the parameters utilized in the model.
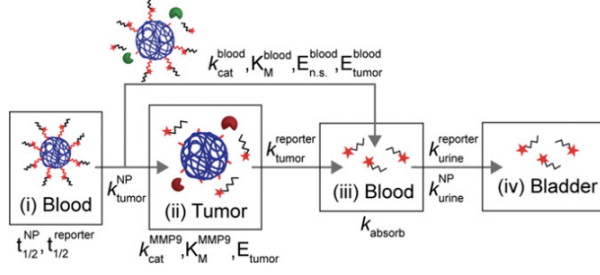
Figure 4: Lumped model for the in vivo pathway of the nanoparticle consisting of four main compartments. Notice that there is an additional pathway attributed for both on and off-target proteolytic cleavage in the plasma. Image courtesy of Kwong *et al*, 2015

The mathematical equations that represent each compartment of the lumped model were derived from both the standard Michaelis-Menten kinetics equation:

$$V_o = \frac{k_2[E_t][S]}{K_m + [S]}$$

in which the conditions of quasi-steady state are assumed, and Fick's law of diffusion:

$$J = -D\frac{d\varphi}{dx}$$

Variable	Description	Unit	Value
τ	constant for NP in plasma	min^{-1}	0.0462
P	permeability constant for tumor	m^{-1}	$2.3 * 10^{-4}$
k_{cat}^{MMP9}	catalytic efficiency of MMP9	min^{-1}	3.99
k_{cat}^{blood}	catalytic efficiency	min^{-1}	0.0659
$k_{tumor}^{reporter}$	rate of reporter diffusion across tumor	min^{-1}	0.09
$k_{urine}^{reporter}$	rate of reporter filtration into urine	min^{-1}	0.032
$k_{MPS}^{reporter}$	rate of reporter clearance by MPS	min^{-1}	0.0064
k_{absorb}	rate of NP and reporter reabsorption	min^{-1}	2.89
K_M^{MMP9}	K_m MMP9 cleavage	M	$2.13 * 10^{-6}$
K_M^{blood}	K_m plasma cleavage	M	$1.0063 * 10^{-5}$
E_{MMP9}^{blood}	concentration of shed proteases in blood	M	$7.1623 * 10^{-8}$
$E_{n.s.}^{blood}$	concentration in blood	M	$4 * 10^{-6}$
E_{MMP9}^{tumor}	concentration of proteases in tumor	M	$7.1624 * 10^{-7}$

Table 1: Parameters

2.1.1 First Compartment: Blood

The first compartment representing the concentration of NPs in the plasma is derived from a series of separate components including its half-life, the diffusion out of the plasma into the tumor, and its enzymatic degradation:

$$dC_{NP_{plasma}} = -\tau * C_{NP_{plasma}} - k_{tumor}^{NP} * (C_{NP_{tumor}} - C_{NP_{plasma}}) - \frac{k_{cat}^{MMP9} * E_{MMP9}^{blood} * C_{NP_{plasma}}}{(K_M^{MMP9} + C_{NP_{plasma}})} - \frac{k_{cat}^{blood} * E_{n.s.}^{blood} * C_{NP_{plasma}}}{(K_M^{blood} + C_{NP_{plasma}})}$$

The first portion of the equation represents the half-life of the NP which negatively affects the concentration in the plasma. The second portion of the equation represents the diffusion of the NP out of the

plasma into the tumor. It is important to note that this type of diffusion equation is typically a function of permeability, surface area, and volume (discussed later in the report), however, it has been replaced by the term k_{tumor}^{NP}. The final portion of this equation depicts the enzymatic degradation from both specific(MMP9) and non-specific proteases in the blood.

2.1.2 Second Compartment: Tumor Bed

The second compartment in the lumped model is comprised of two differential equations describing the concentration of NPs in the tumor and the concentration of reporter in the tumor. Both equations are constructed using a combination of Fick's Law of Diffusion and the Michaelis-Menten equation for enzyme kinetics. The first equation in this compartment assumes that only two dynamic changes govern the change in NP concentration in the tumor: NP diffusion and NP degradation:

$$dC_{NP_{tumor}} = k_{tumor}^{NP} * (C_{NP_{plasma}} - C_{NP_{tumor}}) - \frac{k_{cat}^{MMP9} * E_{MMP9}^{tumor} * C_{NP_{tumor}}}{(K_M^{MMP9} + C_{NP_{tumor}})}$$

The first term in this equation represents the diffusion of the NP from the blood into the tumor bed, and the second term of the equation captures the degradation of the NP due to MMP9 enzyme activity.

The second equation in the tumor compartment describes the concentration of reporter accumulating in the tumor.

$$dC_{R_{tumor}} = \frac{k_{cat}^{MMP9} * E_{MMP9}^{tumor} * C_{NP_{tumor}}}{(K_M^{MMP9} + C_{NP_{tumor}})} - k_{tumor}^{reporter} * (C_{R_{tumor}})$$

The first term in this second equation is the complement of the second term in the first equation, capturing the enzymatic activity of MMP9 on the NP to create free reporter in the tumor. The second term in this second equation represents the diffusion of the reporter out of the tumor and into the surrounding blood. The reporter in the plasma,$C_{R_{plasma}}$, is significantly diluted and cleared rapidly, therefore for simplicity it has been ignored in the second expression of the equation.

2.1.3 Third Compartment: Blood

The third compartment models the concentration of reporter in the plasma; it is constructed from five terms: (i) diffusion of the reporter from the tumor into the plasma, (ii) enzymatic activity of MMP9 in the blood, (iii) enzymatic activity of non-specific proteases in the blood, (iv) clearance of the reporter from kidney filtration and MPS (mononuclear phagocyte system), and (v) absorption of reporter (e.g. from renal tubes).

$$dC_{R_{plasma}} = k_{tumor}^{reporter} * C_{R_{tumor}} + \frac{k_{cat}^{MMP9} * E_{MMP9}^{blood} * C_{NP_{plasma}}}{(K_M^{MMP9} + C_{NP_{plasma}})} + \frac{k_{cat}^{blood} * E_{n.s.}^{blood} * C_{NP_{plasma}}}{(K_M^{blood} + C_{NP_{plasma}})}$$

$$-(k_{urine}^{reporter} + k_{MPS}^{reporter}) * (C_{R_{plasma}}) - k_{absorb} * (C_{R_{plasma}})$$

2.1.4 Fourth Compartment: Bladder

The fourth and final compartment of the model describes the concentration of the reporter in the urine, and it is governed by a single rate equation:

$$dC_{R_{urine}} = k_{urine}^{reporter} * C_{R_{plasma}}$$

2.2 Numerical Solution

Recalling equations (1) and (2), we have placed our focus on this k_{tumor}^{NP} term, the rate of nanoparticle diffusion across tumor vessels. In [6], this term is defined as

$$k_{tumor}^{NP} = \frac{P * S_{tumor}}{V_{tumor}}$$

where S_{tumor} and V_{tumor} are the surface area and volume of the tumor, respectively. Assuming a spherical-shaped tumor, we can then take S_{tumor} and V_{tumor} to be

$$S_{tumor} = 4 * \pi * r^2$$

$$V_{tumor} = \frac{4}{3} * \pi * r^3$$

Thus, our expression for k_{tumor}^{NP} simplifies to

$$k_{tumor}^{NP} = \frac{3 * P}{r}$$

This constitutes our primary modification to the mathematical model utilized by Kwon *et al.* By tuning this parameter based on the radii of tumors of various sizes, we can see the effect of tumor size on concentration of reporter in urine.

The numerical solution to our system of five ODEs was solved computationally using MATLAB and its built-in ODE23 solver. The numerical solution utilizes the ODEs exactly as outlined in [6], with our modification for k_{tumor}^{NP}.

Variable	Description	Initial Conditions [M]
$dC_{NP_{plasma}}$	Nanoparticle in Plasma	$2.5 * 10^{-}6$
$dC_{NP_{tumor}}$	Nanoparticle in Tumor	0
$dC_{R_{tumor}}$	Reporter in Tumor	0
$dC_{R_{plasma}}$	Reporter in Plasma	0
$dC_{R_{urine}}$	Reporter in Urine	0

Table 2: Initial Conditions

Table 2 lists the initial conditions utilized in the ODE23 solver. There is a small amount of nanoparticle initially injected into the bloodstream. All other concentrations are initially at zero. Absolute tolerance and relative tolerance in the mathematical model were set to $1 * 10^{-20}$.

2.3 Analytical Solution

According to Dr. Gert Cauwenberghs no method exists to analytically solve these equations, "except if you're a math wizz of the caliber of Laplace himself and make a breakthrough in solving general nonlinear ODEs..." However, we can look at these ODEs in various domains, which will allow us to simplify the equations into forms more amenable to analytical manipulation. The complete list of equations governing our model is listed below:

1.

$$dC_{NP_{plasma}} = -\tau * C_{NP_{plasma}} - k_{tumor}^{NP} * (C_{NP_{tumor}} - C_{NP_{plasma}}) - \frac{k_{cat}^{MMP9} * E_{MMP9}^{blood} * C_{NP_{plasma}}}{(K_M^{MMP9} + C_{NP_{plasma}})}$$

$$- \frac{k_{cat}^{blood} * E_{n.s.}^{blood} * C_{NP_{plasma}}}{(K_M^{blood} + C_{NP_{plasma}})}$$

2.

$$dC_{NP_{tumor}} = k_{tumor}^{NP} * (C_{NP_{plasma}} - C_{NP_{tumor}}) - \frac{k_{cat}^{MMP9} * E_{MMP9}^{tumor} * C_{NP_{tumor}}}{(K_M^{MMP9} + C_{NP_{tumor}})}$$

3.

$$dC_{R_{tumor}} = \frac{k_{cat}^{MMP9} * E_{MMP9}^{tumor} * C_{NP_{tumor}}}{(K_M^{MMP9} + C_{NP_{tumor}})} - k_{tumor}^{reporter} * (C_{R_{tumor}})$$

4.

$$dC_{R_{plasma}} = k_{tumor}^{reporter} * C_{R_{tumor}} + \frac{k_{cat}^{MMP9} * E_{MMP9}^{blood} * C_{NP_{plasma}}}{(K_M^{MMP9} + C_{NP_{plasma}})} + \frac{k_{cat}^{blood} * E_{n.s.}^{blood} * C_{NP_{plasma}}}{(K_M^{blood} + C_{NP_{plasma}})}$$

$$-(k_{urine}^{reporter} + k_{MPS}^{reporter}) * (C_{R_{plasma}}) - k_{absorb} * (C_{R_{plasma}})$$

5.

$$dC_{R_{urine}} = k_{urine}^{bladder} * C_{R_{plasma}}$$

We first observe that equations (1) and (2) are coupled. Our method of choice to uncouple the two variables, $C_{NP_{plasma}}$ and $C_{NP_{tumor}}$, would be Laplace. However, the variables in the denominator of the fractions make these equations unamenable to the Laplace method. If we look at these equations in domains defined by the rate constants in the denominators of these terms (Figure 5), we can simplify the equations to a form that is solvable using Laplace. If we assume that the conentration of nanoparticle in the blood ($C_{NP_{plasma}}$) is much smaller than the Michaelis Menten contant for MMP9 (K_M^{MMP9}), and that the concentration of nanopartible in the tumro ($C_{NP_{tumor}}$) is much smaller than K_M^{MMP9} we can cancel out the $C_{NP_{plasma}}$ term in the denominator of equations (1) and (4) and the $C_{NP_{tumor}}$ term in the denominator of equations (2) and (3). This restricts our analysis to the domain highlighted below in Figure 5,
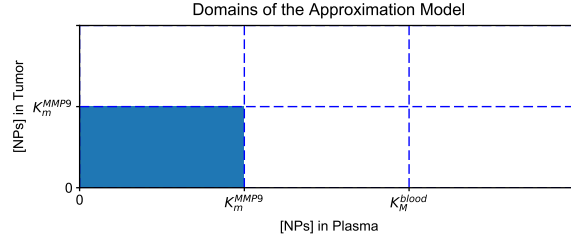

Figure 5: Equations 1 and 2 separated into domains based on the rate constants $K_{M MMP9}$ and $K_{M blood}$

After making these assumptions our equations simplify to the following forms below. Biologically, the concentration of nanoparticle in the blood and plasma is close to the $K_{M MMP9}$ value, therefore to complete our model, our next step was to make similar assumptions to solve for the two subsequent domains at which the $K_M^{MMP9} < C_{NP_{plasma}} < K_M^{blood}$ and $C_{NP_{tumor}} > K_M^{blood}$. However, our analytical results for the first domain (see Results section) failed to give us conclusive evidence that our assumptions logically modeled any biologically relevant characteristics. Therefore, we decided to disregard our analytical methods and to focus on the numerical solutions.

1.

$$dC_{NP_{plasma}} = -\tau * C_{NP_{plasma}} - k_{tumor}^{NP} * (C_{NP_{tumor}} - C_{NP_{plasma}}) - \frac{k_{cat}^{MMP9} * E_{MMP9}^{blood} * C_{NP_{plasma}}}{K_M^{MMP9}}$$

$$-\frac{k_{cat}^{blood} * E_{n.s.}^{blood} * C_{NP_{plasma}}}{K_M^{blood}}$$

2.

$$dC_{NP_{tumor}} = k_{tumor}^{NP} * (C_{NP_{plasma}} - C_{NP_{tumor}}) - \frac{k_{cat}^{MMP9} * E_{MMP9}^{tumor} * C_{NP_{tumor}}}{K_M^{MMP9}}$$

3.

$$dC_{R_{tumor}} = \frac{k_{cat}^{MMP9} * E_{MMP9}^{tumor} * C_{NP_{tumor}}}{K_M^{MMP9}} - k_{tumor}^{reporter} * (C_{R_{tumor}})$$

8

4.

$$dC_{R_{plasma}} = k_{tumor}^{reporter} * C_{R_{tumor}} + \frac{k_{cat}^{MMP9} * E_{MMP9}^{blood} * C_{NP_{plasma}}}{K_M^{MMP9}} + \frac{k_{cat}^{blood} * E_{n.s.}^{blood} * C_{NP_{plasma}}}{K_M^{blood}}$$

$$-(k_{urine}^{reporter} + k_{MPS}^{reporter}) * (C_{R_{plasma}}) - k_{absorb} * (C_{R_{plasma}})$$

5.

$$dC_{R_{urine}} = k_{urine}^{bladder} * C_{R_{plasma}}$$

These 5 equations are now easier to work with, allowing us to use the Laplace method to arrive at an analytical solution for our model. Laplace transform was performed on the coupled equations (1) and (2). The resulting equations are shown below.

$$C_a = -\tau * -k_{tumor}^{NP} - \left(\frac{k_{cat}^{MMP9} * E_{MMP9}^{blood}}{k_M^{MMP9}} \right) - \left(\frac{k_{cat}^{blood} * E_{n.s.}^{blood}}{k_M^{blood}} \right)$$

$$C_b = K_{tumor}^{NP} - \frac{k_{cat}^{MMP9} * E_{MMP9}^{tumor}}{K_M^{MMP9}}$$

$$A(s) = \frac{a_o s + C_b a_o}{s^2 + C_b s - (C_a + C_a C_b C_1)}$$

$$B(s) = \frac{k_{tumor}^{NP} * a_o}{s^2 + (C_b - C_a)s - (C_a C_b + C_1)}$$

After we took into account the permeability, volume, and surface area of the tumor by replacing the NP rate of diffusion constant, we decided to explore additional parameters that may be influenced by tumor size. The original equations only considered the volume and surface area of the tumor in relation to the diffusion of NP into the tissue. Logically, we expect that the concentration of reporter that diffuses out of the tumor is also dependent on its size. Thus, we substituted the same equation (3*P/r) with the reporter rate of diffusion constant in equations (3) and (4).

3 Results

3.1 Numerical Solution

We ran our mathematical model over a range of tumor radii (0.001mm - 5mm) and plotted the resulting reporter concentration in urine over time, seen below in Figure 6.
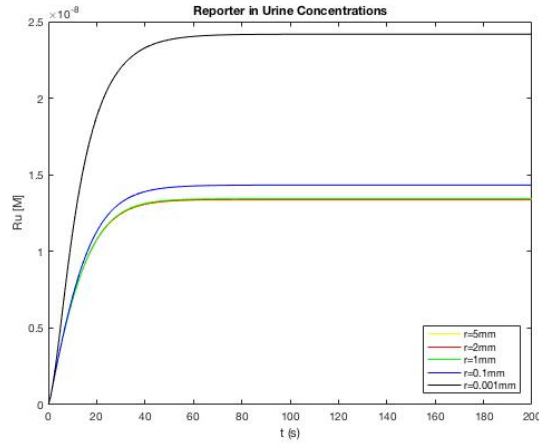

Figure 6: Reporter Concentration in Urine Over Time.

The model indicates that with increasing tumor radius, the reporter concentration in urine decreases. We then plotted the steady state concentration of reporter in urine against radius, which confirms this phenomenon.
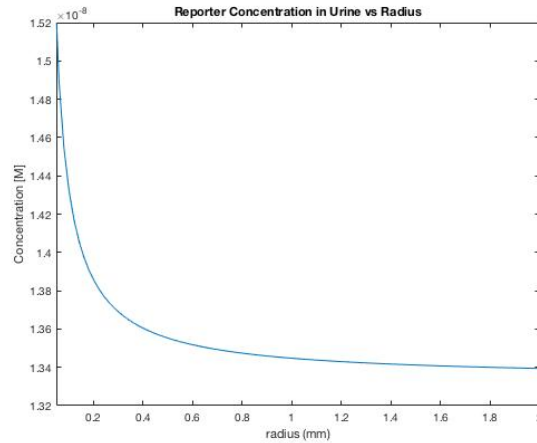

Figure 7: Reporter Concentration in Urine Versus Radius.

This is contrary to our initial hypothesis that the amount of reporter in urine would increase with increasing tumor radius. One possible biological explanation for this phenomenon involves the surface area to volume ratio in cells. As a cell (tumor in this case) grows, its surface area does not increase linearly compared to its volume. The volume increases much more rapidly than the surface area. At significantly large sizes, the cell will reach a point where substances cannot enter or leave the cell in a sufficient amount of time. Thus at large sizes, the concentration of reporter leaving the tumor and entering the blood and urine assymptotically approaches a constant value.
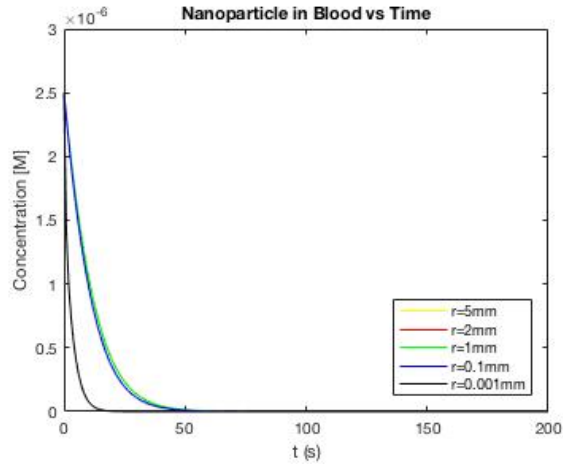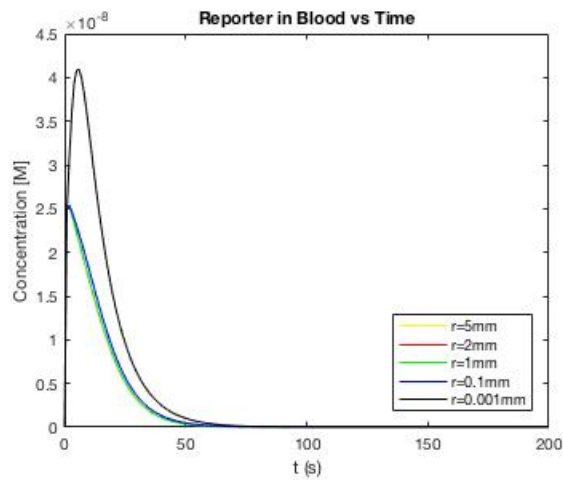
(a) Nanoparticle in Blood.
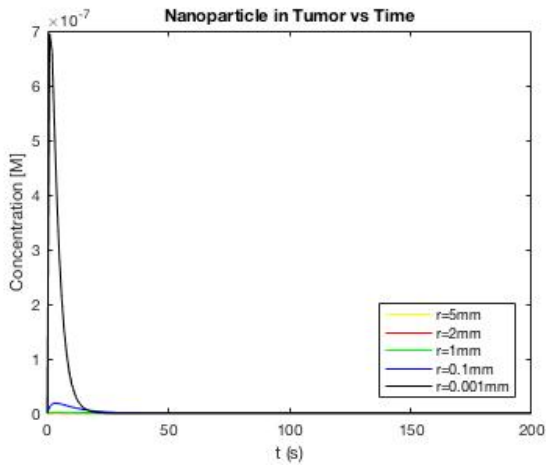
(b) Nanoparticle in Tumor.
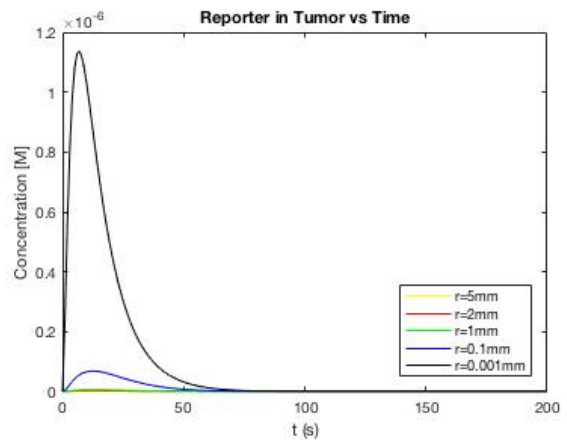
(c) Reporter in Tumor.

(d) Reporter in Blood.

Figure 8: Nanoparticle and Reporter Concentrations in Blood and Tumor.

Figure 8 shows the numerical solutions for the remaining set of ODEs, using various radii values. These

11

results further contribute to the phenomenon described above. At all radii there is an initial concentration of nanoparticle in the blood. The nanoparticle diffuses into the tumor, arriving at a significantly higher concentration in smaller radii than in larger radii, possibly due to the surface area-to-volume ratio described earlier. This consequently leads to the levels of reporter seen in the tumor and the blood, leading to the final reporter concentration in urine seen in Figure 6 and Figure 7.

After observing that the concentration of reporter in the urine is inversely proportional to tumor size, we decided to alter an additional parameter, the rate constant for the diffusion of the reporter out of the tumor ($k_{tumor}^{reporter}$). Loginally, one would expect the tumor size to affect the rate at wich the reporter diffuses out of the tumor. Because this term is analogous to k_{tumor}^{NP} (the rate at which the nanoparticle diffuses into the tumor), the two terms now have equivalent definitions.

$$k_{tumor}^{NP} = \frac{3 * P}{r} = k_{tumor}^{reporter}$$

This adjustment caused the relative concentration of reporter in the urine to increase with radius size (Figure 9). However, we noticed that when the radius drops below 1mm, the model fails to capture the same trend.
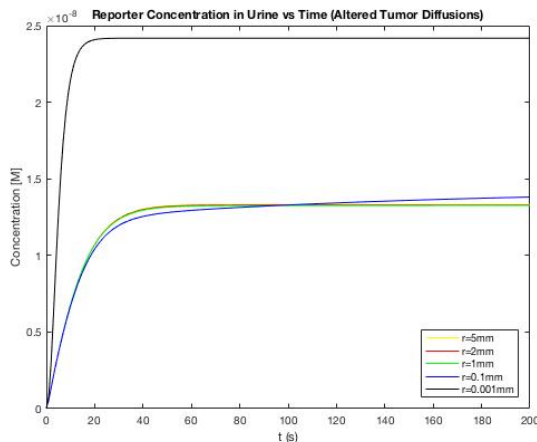

Figure 9: Updated model for the concentration of reporter in the urine taking into account additional parameters affected by tumor size.

Thus, we decided to consider our model only with tumors that have a radius larger than 1mm (Figure 10). After filtering out these limitations from our data set, the model becomes biologically significant; as the radius of the tumor shrinks, there is less reporter collected in the urine. Biologically, a smaller tumor will lessen the amount of NP that can successfully diffuse into the tissue ultimately limiting the amount of reporter that is cleaved and filtered into the urine.
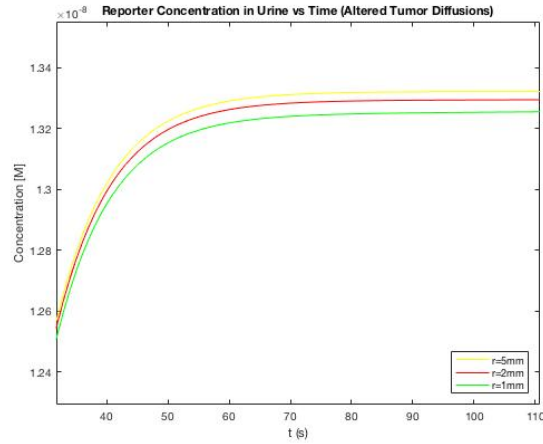
Figure 10: Updated model for the concentration of reporter in the urine while considering additional parameters affected by tumor size.

3.2 Analytical Solution

After making the assumption that our concentration of NP in the blood and tumor was low in relation to the Km of the tumor-associated MMP9, we were able to simplify the system of equations allowing us to solve it by hand. We graphed the first compartment of the Laplace approximation which was representative of a dampened sinusoidal function. Upon further observation, we realized that each subsequent peak of the function exponentially decreased. After overlaying the original ODE for the blood compartment, we saw that the dampened sine wave captured the general trend of the original ODEs (Figure 11).
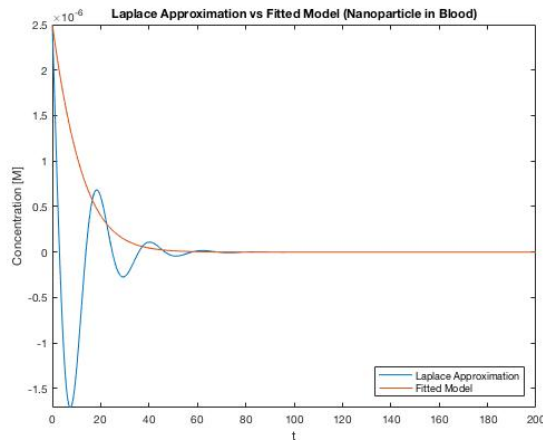

Figure 11: Laplace Approximation of of the first compartment in the lumped model, representing the concentration of NPs over time. The original ODE model was superimposed over the plot for comparison. Graph created using MATLAB for students.

3.3 Summary

In summary, we modified a pre-exsting mathematical model [16] to predict tumor size based upon the concentration of a cleavable reporter found in the urine. We modified two rate constants that govern the diffusion of NP into the tumor and the diffusion of reporter out of the tumor. Our initial attempts at arriving at an analytical solution were not biologically significant. For these reasons, we focused on solving

our model of ODEs with numerical methods. This produced a model which supported our hypothesis that the concentration of reporter in the urine is dependent on tumor size. Our solution proved biologically significant for tumors with a radius larger than 1mm; otherwise the results deviate from the exptected trend.

Previous studies focused solely on tumor detection rather than quantification [15][16]. Our model provides a novel approach in correlating reporter concentration in the urine and tumor size for use as an early detection and diagnostic tool. Alternative methods for detecting tumors include various screening protocols which often result in false-positive and false-negative results [18]. Our adapted model provides clinical implications as a more accurate tumor screening protocol in early cancer detection.

4   Future Work

We must consider several limitations to our current model. First, our analytical approximation only reflects low concentrations of NPs in the blood and tumor with respect to the Km of MMP9 in the tumors. Realistically, the concentration of NP in the blood and tumor is close to the Km of MMP9 [15], so we need to adapt our approximation to also include a domain that extends into the region at which our NP concentration is close to the Km of MMP9 in the tumor. Our second limitation arises from the possibility that additional rate constants may be dependent on the tumor size. Our numerical model only takes into accound tumor size affects on the rate constant associated with the diffusion of NPs into the tumor and the rate of reporter diffusion out of the tumor. The third limitation includes our inablilty to accurately model the expected behavior of tumors smaller than 1mm.

Taking these limitations into account, our future directions include determining all of the variables that are dependent on tumor size and incorporating these into the model. This would improve the accuracy of our current numerical solution. In order to produce a more accurate analytical model, we need to incorporate additional domains such as when the concentration of NPs in the blood is close to the Km of the MMP9 in the tumors. Finally, given the observation that MMP9 is expressed at varying levels across different cancer types, we would like to determine if the model can be used to diagnose tumor type based on MMP9 activity. We would approach this by using known expression levels of the enzyme (Figure 2) and use our model to calculate expected reporter output in the urine based on cancer type.

References

[1] Cancer Statistics [Internet]. National Cancer Institute. 2017 [cited 2017 Oct 31];Available from: https://www.cancer.gov/about-cancer/understanding/statistics

[2] Statistics for Different Kinds of Cancer [Internet]. Centers for Disease Control and Prevention. 2017 [cited 2017 Oct 31];Available from: https://www.cdc.gov/cancer/dcpc/data/state.htm

[3] Etzioni, R. *et al.* The case for early detection. *Nat. Rev.* Cancer 3, 243–252 (2003).

[4] *SEER Cancer Statistics Review, 1975-2013* (National Cancer Institute, 2016); $http : seet.cancer.gov/csr/1975_2013$

[5] Kanas, G. P. *et al.* Survival after liver resection in metastatic colorecal cancer: review and meta-analysis of prognostic factors. *Clin. Epidemiol.* 4, 283-301 (2012)

[6] Eveleth R. There are 37.2 Trillion Cells in Your Body [Internet]. Smithsonian.com. 2013 [cited 2017 Oct 31];Available from: https://www.smithsonianmag.com/smart-news/there-are-372-trillion-cells-in-your-body-4941473/

[7] Hanahan D, Weinberg RA. Hallmarks of Cancer: The Next Generation. *Cell* 2011;144(5):646–74.

[8] Biomarkers [Internet]. National Tay-Sachs & Allied Diseases Association. [cited 2017 Nov 3];Available from: https://www.ntsad.org/index.php/resources/glossary/76-biomarkers

[9] Sawyers CL (2008) The cancer biomarker problem. *Nature* 452(7187):548–552.

[10] La Thangue NB, Kerr DJ (2011) Predictive biomarkers: A paradigm shift towards personalized cancer medicine. *Nat Rev Clin Oncol* 8(10):587–596.

[11] Fader, A. N. *et al.* The prognostic significance of pre- and post-treatment CA-125 in grade 1 serous ovarian carcinoma: a gynecologic Oncology Group study. *Gynecol. Oncol.* 132, 560-565 (2014)

[12] Frangioni, J. C. New technologies for human cancer imaging. *J. Clin. Oncol.* 26, 4012-4021 (2008)

[13] Hori, S. S. & Gambhir, S. S. Mathematical model identifies blood biomarker-based early cancer detection strategies and limitations. *Sci. Transl.* Med. 3, 109ra116 (2011)

[14] Henry, N. L. & Hayes, D.F. Cancer biomarkers. *Mol. Oncol.* 6, 140-146 (2012)

[15] Kwon, E. *et al.* (2017). Ultrasensitive tumor-penetrating nanosensors of protease activity. *Nature Biomedical Engineering.* 10.1038.

[16] Kwong, G. *et al.*(2015). Mathematical framework for activity-based cancer biomarkers. *PNAS.* 112(41). 10.1073

[17] https://www.ncbi.nlm.nih.gov/books/NBK21590/

[18] https://www.cancer.gov/about-cancer/screening

5 Appendix

5.1 Matlab Code: Solving ODEs

```
function [t,Ru,Np,Nt,Rt,Rp]=rr(r)
% INPUTS: r - tumor size (mm)
% look in model() below for ENZYME FOR E_MMP9_TUMOR

%Original description of model from Kwong et al., PNAS (2015), 112(41):12627.
%Constants taken from Kwong et al., unless noted

% Calls the ODE function below  over 200 minutes with the initial
% concentration in the blood of 2.5 uM and 0 uM everywhere else
options = odeset('AbsTol',1e-20,'RelTol',1e-20);
%[t,y] = ode15s(@(t,y) model(t,y),0:200, [2.5e-6, 0, 0,0, 0.001],options);

[t,y] = ode23(@(t,y) model(t,y,r),0:200, [2.5e-6, 0, 0,0, 0],options);

%Tumor bearing values from ODE
Np=y(:,1); %Nanoparticle in plasma
Nt=y(:,2); %Nanoparticle in tumor
Rt=y(:,3); %Reporter in tumor
Rp=y(:,4); %Reporter in plasma
Ru=y(:,5); %Reporter in urine

function dydt = model(t,y,r)

%clearing constants
mps_np = 4.62e-02; %m^-1 [[k_MPS]] . Reflect clearance rate from Kwon/Dudani et al.
mps_r = 0.0064; %m^-1 Reporter clearance
k_np_filter = 1.66e-05; %m^-1 Urinary filtration of NP
k_r_filter = 0.032; %m^-1 Urinary filtration of reporter
k_absorb = 2.89; % [M]/min Fit to account for reporter loss.

%permeability constants
%p_np_tissue = 1.4e-04; %m^-1 Transport of NP into tumor. 1.18 term from improved accumulation (Fig. 2, %Kwon/Dudani et al.).
p_r_tissue = 0.09; %m^-1 Transport of reporter

%%%%%%%%%%%%%%%%%%%%%%%%%%%%%% K VALUE %%%%%%%%%%%%%%%%%%%%%%%%%%%%%%%%%%%%%%%
p_np_tissue = 3 * 2.3e-4 / r;

%%%PLASMA
%plasma enzyme kinetic constants
k_cat_bckg = 0.0659/29.5; % [1/min] Plasma cleavage Kcat. 29.5 term from decreased thrombin cleavage
k_m_bckg = 1.0063e-05; % [M] Plasma cleavage Km

%TUMOR
%tumor enzyme kinetic constants
k_cat = 0.5*3.99; % [1/min] MMP9 cleavage kcat. 3.99 term from increased MMP9 cleavage (Fig. 2, Kwon/Dudani et al.).
k_m = 2.13e-06; % [M] MMP9 cleavage Km

%enzymes
e_nonspecific = 4e-6; % [M]
e_plasma = 7.1623e-8;% [M] Plasma = 1/10th [Tissue], see Hori et al., STM (2011), 3(109):109.

e_tissue = 7.1624e-7; % [M]  %% ORIGINAL VALUE FOR e_tissue  (need to
%e_tissue = 0;
% write a function) - applies to 5mm


%%%%State Conditions
C_np_plasma = y(1);
C_np_tissue = y(2);
C_r_tissue = y(3);
C_r_plasma = y(4);
C_r_urine = y(5);
```

```
%Nanoparticle concentration in plasma: function of circulation time, clearance into
%tumor, cleaving due to free, nonspecific proteases, and cleaving due to secreted
%enzymes from tumor
dC_np_plasmadt = -(mps_np+k_np_filter)*C_np_plasma - (p_np_tissue*(C_np_plasma-C_np_tissue))-
(k_cat_bckg*e_nonspecific*C_np_plasma)/(k_m_bckg+C_np_plasma) - (k_cat*e_plasma*C_np_plasma)/(k_m+C_np_plasma);

%Nanoparticle concentration in tissue: function of clearance into
%tumor and cleaving due to secreted enzymes
dC_np_tissuedt = (p_np_tissue*(C_np_plasma-C_np_tissue))- (k_cat*e_tissue*C_np_tissue)/(k_m+C_np_tissue);

%Reporter concentration in tissue: function of cleaving of nps and clearance into
%blood
dC_r_tissuedt =(k_cat*e_tissue*C_np_tissue)/(k_m+C_np_tissue) - (p_r_tissue*(C_r_tissue));

%Reporter concentration in plasma: function of clearance into blood from
%tissue, natural decay, and cleavage in blood of np, and clearance into
%urine
dC_r_plasmadt = (p_r_tissue*(C_r_tissue)) - (k_r_filter+mps_r+k_absorb)*C_r_plasma +

(k_cat_bckg*e_nonspecific*C_np_plasma)/(k_m_bckg+C_np_plasma) + (k_cat*e_plasma*C_np_plasma)/(k_m+C_np_plasma);

%reporter concentration in urine: function of clearance into urine from
%blood
dC_r_urinedt = k_r_filter*(C_r_plasma);

dydt = [dC_np_plasmadt; dC_np_tissuedt; dC_r_tissuedt; dC_r_plasmadt; dC_r_urinedt];
return
```

5.2   Matlab Code: Utilizing ODE Solver and Plotting

```
[t,Ru1,Np1,Nt1,Rt1,Rp1] = rr(5);
[t2,Ru2,Np2,Nt2,Rt2,Rp2] = rr(2);
[t3,Ru3,Np3,Nt3,Rt3,Rp3] = rr(1);
[t4,Ru4,Np4,Nt4,Rt4,Rp4] = rr(0.1);
[t5,Ru5,Np5,Nt5,Rt5,Rp5] = rr(0.001);

figure
plot(t,Ru1,'y')
hold on
plot(t2,Ru2,'r')
plot(t3,Ru3,'g')
plot(t4,Ru4,'b')
plot(t5,Ru5,'k')
xlabel('t (s)')
ylabel('Concentration [M]')
legend('r=5mm','r=2mm','r=1mm','r=0.1mm','r=0.001mm','Location','Southeast')
title('Reporter Concentration in Urine vs Time')

figure
plot(t,Np1,'y')
hold on
plot(t2,Np2,'r')
plot(t3,Np3,'g')
plot(t4,Np4,'b')
plot(t5,Np5,'k')
xlabel('t (s)')
ylabel('Concentration [M]')
legend('r=5mm','r=2mm','r=1mm','r=0.1mm','r=0.001mm','Location','Southeast')
title('Nanoparticle in Blood vs Time')

figure
plot(t,Nt1,'y')
hold on
plot(t2,Nt2,'r')
plot(t3,Nt3,'g')
plot(t4,Nt4,'b')
plot(t5,Nt5,'k')
```

```
xlabel('t (s)')
ylabel('Concentration [M]')
legend('r=5mm','r=2mm','r=1mm','r=0.1mm','r=0.001mm','Location','Southeast')
title('Nanoparticle in Tumor vs Time')

figure
plot(t,Rt1,'y')
hold on
plot(t2,Rt2,'r')
plot(t3,Rt3,'g')
plot(t4,Rt4,'b')
plot(t5,Rt5,'k')
xlabel('t (s)')
ylabel('Concentration [M]')
legend('r=5mm','r=2mm','r=1mm','r=0.1mm','r=0.001mm','Location','Southeast')
title('Reporter in Tumor vs Time')

figure
plot(t,Rp1,'y')
hold on
plot(t2,Rp2,'r')
plot(t3,Rp3,'g')
plot(t4,Rp4,'b')
plot(t5,Rp5,'k')
xlabel('t (s)')
ylabel('Concentration [M]')
legend('r=5mm','r=2mm','r=1mm','r=0.1mm','r=0.001mm','Location','Southeast')
title('Reporter in Blood vs Time')
```